Liquid−Gas Transitions in Charged Colloidal Dispersions: Small-Angle Neutron Scattering Coupled with Phase Diagrams of Magnetic Fluids

E. Dubois,*,† R. Perzynski,‡ F. Boué,§ and V. Cabuil†

Laboratoire Liquides Ioniques et Interfaces Chargées, CNRS UMR 7612, Casier 63, Université Pierre et Marie Curie, 4 place Jussieu, 75252 Paris Cedex 05, France, Laboratoire des Milieux Désordonnés et Hétérogènes, CNRS UMR 7603, Casier 78, Université Pierre et Marie Curie, 4 place Jussieu, 75252 Paris Cedex 05, France, and Laboratoire Léon Brillouin, CEA-CNRS, CE Saclay, 91191 Gif-sur-Yvette, France

Received January 18, 2000. In Final Form: April 13, 2000

We study here the phase behavior of colloidal dispersions, which are constituted of almost monodisperse γ-Fe_2O_3 magnetic nanoparticles dispersed in water at pH 7. Those electrostatically stabilized dispersions present, if the interparticle repulsion is decreased, gas−liquid transitions, a phase behavior scarcely reported for such charged nanoparticles. Small-angle neutron scattering experiments prove that there is no chaining of the particles and that, from the point of view of interparticle interactions, increasing ionic strength (through addition of NaCl) is equivalent to decreasing temperature. A phenomenological expression of the osmotic pressure π is determined and shown to be in agreement with direct π measurements. The scattering experiments associated to optical microscopy determinations of phase diagrams lead to a general $\pi-\Phi$ diagram. Gas−solid transitions may exist even if their observation is disturbed by metastability phenomena. The results are in qualitative agreement with theoretical predictions on charged colloids and in agreement with theoretical works on weak dipolar systems.

1. Introduction

A major preoccupation concerning colloidal solutions, which are dispersions of solid particles in a liquid, is their stabilization. Indeed, the van der Waals attractions between particles have to be counterbalanced by repulsion in order to avoid the aggregation of particles.[1] Colloidal solutions can be modeled as dispersions of large objects (the particles) in a continuous medium (the solvent) and they present therefore strong analogies with a simple atomic system. Moreover, the effective interaction potential between particles is usually qualitatively similar to the Lennard-Jones potential between atoms. Colloidal solutions should thus lead to the same kind of phase diagrams as atomic systems: gas, liquid, fluid, and solid phases should exist. The osmotic pressure π replaces the pressure P and the volume fraction of particles Φ replaces the volume V. The diagram $\pi-\Phi$ thus replaces the standard diagram $P-V$.[2] The gas phase corresponds to a solution of low volume fraction, the liquid phase corresponds to a dense but not organized solution, and the crystal phase is an organized solid phase.

However, colloidal dispersions differ from atomic systems in some aspects. First, as the osmotic pressure is more difficult to measure than the pressure P, this $\pi-\pi$ diagram is experimentally difficult to build directly. Second, contrary to atomic systems, the particles are usually polydisperse, a situation that has a deep influence on the phase diagrams, making difficult the comparison with theoretical studies, which almost always deal with monodisperse systems. Moreover, polydispersity itself, if large enough, may lead to phase separations due to depletion phenomena, which have been studied both theoretically[3,4] and experimentally.[5,6] Third, the interparticle interactions depend on many parameters and phase diagrams are thus often plotted as a function of these parameters (ionic strength, noninteracting added polymer, temperature, etc.).

As the interparticle potential may be controlled in strength and range in some colloidal systems, the study of the influence of the potential on the behavior of colloidal dispersions is experimentally possible. According to recent theoretical works,[7] the $\pi-\Phi$ diagram predicted depends on the range of attraction compared to the range of repulsion. If attractions are long ranged, a gas−liquid−solid diagram like the schematic one plotted in Figure 1 is obtained. A critical point exists (T_c), as well as a triple point (T_p) and gas−liquid transitions are observed for $T < T_c$. For $T > T_c$, only fluid−solid transitions occur for high Φ. If the range of attractive interactions is shorter, T_c becomes smaller than T_p and the liquid does not exist: it is a fluid−solid diagram.[7] If many experimental works deal with fluid−solid diagrams,[2] many fewer works deal with gas−liquid−solid phase diagrams. The studies can be separated according to the nature of repulsion between particles: steric due to polymers or surfactant chains adsorbed on the particles, or electrostatic due to surface charges on the particle surface. Sterically stabilized

* Author to whom correspondence should be sent.
† Laboratoire Liquides Ioniques et Interfaces Chargées, Université Pierre et Marie Curie.
‡ Laboratoire des Milieux Désordonnés et Hétérogènes, Université Pierre et Marie Curie.
§ Laboratoire Léon Brillouin, CEA-CNRS.

(1) Hunter, R. J. in *Foundations of colloid Science*; Oxford Science Publications: Oxford, 1989.
(2) Pusey, P. N. In *Liquides, cristallisation et transition vitreuse*, Les Houches, 1991; Session LI, Part II, p 767.
(3) Mao, Y.; Cates, M. E.; Lekkerkerker, H. N. W. *Physica A* **1995**, *10*, 222.
(4) Biben, T.; Hansen, J. P. *Phys. Rev. Lett.* **1991**, *66*, 2215.
(5) Sanyal, S.; Easwar, N.; Ramaxwany, S.; Sood, A. K. *Europhys. Lett.* **1992**, *18*, 107−110.
(6) Lekkerkerker, H. N. W.; Dhont, J. K. G.; Verduin, H.; Smits, C.; van Duijneveldt, J. S. *Physica A* **1995**, *213*, 18−29.
(7) Tejero, C. F.; Daanoun, A.; Lekkerkerker, H. N. W.; Baus, M. *Phys. Rev. Lett.* **1994**, *73*, 752.

10.1021/la000053u CCC: $19.00
Published on Web 06/03/2000

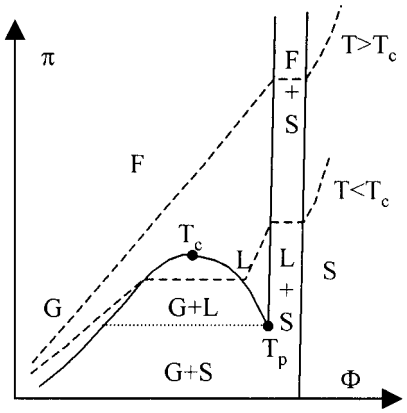

Figure 1. (a) Schematic $\pi-\Phi$ theoretical diagram from ref 2 for a colloidal solution that presents gas, solid, and liquid phases: G = gas, L = liquid, S = solid, F = fluid; T_c, critical point; T_p, triple point. The dashed lines represent two isotherms.

particles have been theoretically[8−10] and experimentally studied.[11−14] Phase transitions may be induced by decreasing temperature or by adding a nonadsorbing polymer that will induce effective interparticle attractions. As the range of the attractions depends on the size of the polymer, it thus allows varying the range of attractions relative to the range of repulsion, i.e., to obtain a fluid−solid phase diagram or a gas−liquid−solid one, as predicted by theory. For electrostatically stabilized particles, Victor and Hansen[15] theoretically studied charged colloids modified by addition of a 1:1 electrolyte. Their predictions depend on the strength of both van der Waals attractions and electrostatic repulsion: reversible gas−liquid transitions occur in a range of parameters all the more narrow as the attraction is larger, otherwise irreversible coagulation is observed. Here again, the nature of the phases obtained depends on the balance between attractions and repulsions. The liquid phase exists in a narrow range of parameters. As far as we know, except studies with ferrofluids, no experimental work reports such gas−liquid transitions with electrostatically stabilized nanoparticles.

Indeed, the colloidal dispersions under study in this paper belong to the class of *electrostatically stabilized nanoparticles* that present gas−liquid-like transitions. They have been described a long time ago with polydisperse particles,[16] and later, identical phenomena have been observed with almost monodisperse particles of various sizes, thus providing evidence that these transitions do not result from depletion due to size polydispersity.[17]

The dispersions considered here are constituted of maghemite γ-Fe_2O_3 nanoparticles dispersed in water and are usually called ionic ferrofluids.[18] In this system, the repulsion between particles is electrostatic, i.e., due to charges at the surface of the particles. They counterbalance van der Waals attractions and magnetic interactions, globally attractive. However, given the nanoparticle sizes and the volume fractions used in the present work, this magnetic interaction is small as compared to van der Waals attractions, even if a magnetic field is applied.[19] We focus here on the behavior without field, and a study under an applied magnetic field will be presented in a forthcoming paper.

In the present article, we study the transitions observed in ionic ferrofluids constituted of almost monodisperse particles of maghemite, in the regime of low volume fractions ($\Phi < 5\%$). The parameters which were varied in order to modify the interparticle potential are the ionic strength (added NaCl) and the temperature. First, the one-phase region is studied through small-angle neutron scattering (SANS) experiments that allow following the evolution of the interparticle interaction until the threshold of destabilization. We show that an experimental expression for the osmotic pressure can be determined from these measurements. Second, above destabilization, macroscopic phase diagrams are built as a function of ionic strength and temperature. Finally, the association of the scattering results and macroscopic phase diagrams leads to the building of a $\pi-\Phi$ phase diagram.

2. Materials and Experiments

2.1. Synthesis and Characterization of Ferrofluids. The particles are chemically synthesized in water by coprecipitation of $FeCl_2$ and $FeCl_3$ in an alkaline solution.[19,20] It leads to γ-Fe_2O_3 magnetic particles, dispersed in an acidic aqueous medium (pH ∼2). Their surface is then coated with trisodium citrate molecules, and the pH of the solution is set to 7.[21] The particle surface charge, which is negative and neutralized by Na^+ counterions, ensures mutual repulsion, prevents flocculation, and thus leads to a stable dispersion in water.

The aqueous ferrofluids used here are characterized by several parameters. The volume fraction Φ of the particles is determined from chemical titration of iron[22] or by absorption spectroscopy at $\lambda = 480$ nm. The particle size distribution is extracted from the magnetization curves. Indeed, as the particles are magnetic monodomains free to rotate in the suspension, the solutions present a giant paramagnetism. If the particles are dilute enough ($\Phi <$ 1%), they may be considered as independent (no interactions between particles) and the magnetization curve of monodisperse particles follows the Langevin formalism, which is strongly size dependent.[18,23] Classically, the size distribution of iron oxide particles is well described by a log-normal distribution of the particles diameter d[18,24]

$$f(d) = \frac{1}{(2\pi)^{1/2}\sigma d}\exp\left[-\frac{1}{2\sigma^2}\left(\ln\frac{d}{d_o}\right)^2\right] \qquad (1)$$

(8) Jansen, J. W.; de Kruif, C. G.; Vrij, A. *J. Colloid Interface Sci.* **1986**, *114*, 471.
(9) Vincent, B.; Edwards, J.; Emmett, S.; Croot, R. *Colloids Surf.* **1988**, *31*, 267
(10) Lekkerkerker, H. N. W.; Ponn, W. C. K.; Pusey, P. N.; Stroobants, A.; Warren, P. B. *Europhys. Lett.* **1992**, *20*, 559.
(11) Jansen, J. W.; de Kruif, C. G.; Vrij, A. *J. Colloid Interface Sci.* **1986**, *114*, 481.
(12) Woutersen, A. T. J. M.; May, R. P.; de Kruif, C. G. *J. Colloid Interface Sci.* **1992**, *151*, 410.
(13) Gast, A. P.; Russel, W. B.; Hall, C. K. *J. Colloid Interface Sci.* **1986**, *109*, 161.
(14) Ilett, S. M.; Orrock, A.; Poon, W. C. K.; Pusey, P. N. *Phys. Rev. E* **1995**, *51*, 1344.
(15) Victor, J. M.; Hansen, J. P. *J. Chem. Soc., Faraday Trans.* **1985**, *2*, *81*, 43−61.
(16) Bacri, J. C.; Perzynski, R.; Salin, D.; Cabuil, V.; Massart, R. *J. Colloid Interface Sci.* **1989**, *132*, 43.
(17) Massart, R.; Dubois, E.; Cabuil, V.; Hasmonay, E.; Perzynski, R. *J. Magn. Magn. Mater.* **1995**, *149*, 1−5.
(18) *Magnetic fluids and Applications Handbook*; Berkovski, Ed.; Begell House Inc. Publ.: New York, 1996.
(19) Dubois, E. Thesis of the University Paris VI, Paris, 1997.
(20) Massart, R. *IEEE Trans. Mag.* **1981**, MAG-17, 1247. Massart, R. French Patent 79-188-42, 1979; U.S. Patent 4329241, 1982.
(21) Dubois, E.; Cabuil, V.; Boué, F.; Perzynski, R. *J. Chem. Phys.* **1999**, *111*, 7147.
(22) Charlot, G. In *Les méthodes de la chimie analytique*; Masson et Cie, ed: Paris, 1966; p 737.
(23) Chantrell, R. W.; Popplewell, J.; Charles, S. W. *Physica* **1977**, *86−88B*, 1421.
(24) Bacri, J. C.; Perzynski, R.; Salin, D.; Cabuil, V.; Massart, R. *J. Magn. Magn. Mater.* **1986**, *62*, 36.

Table 1. Characteristics of the Studied Samples[a]

	A	B	C
d_o (nm)	7.1	8.5	9.5
σ	0.15	0.15	0.2
V_w (10^5 Å^3)	3	7.35	11
A_2 (10^{-6} mol·cm^3·g^{-2})	3.6	1.5	0.7

[a] d_o and σ characterize the size distribution (see text for details), V_w is a weight average of the particle volume determined from SANS, A_2 is the second virial coefficient at $T = 30$ °C without added salt.

where σ is the width of the distribution and $\ln(d_o)$ is the average of $\ln(d)$. A two-parameter fit of the experimental magnetization curves allows d_o and σ to be determined.[24] As the initial size distribution of the dispersed particles is very wide, i.e., it ranges from 3 to 15 nm, a size sorting is performed, leading to a thinner size distribution.[17] The size characteristics of the ferrofluid samples prepared for this study are given in Table 1.

The measurement of the surface charge of the particles[21] (coated with citrate molecules) leads to a maximum value around 2 ± 0.2 charges per nm^2. For all samples studied here, the conditions are set to obtain this maximum value as the superficial charge. The adsorbed citrate is in equilibrium with citrate molecules in the solution, with a typical concentration around 0.04 mol/L in our samples. This leads to a strong initial ionic strength $I = 0.5\sum_i c_i z_i^2$, where c_i and z_i are the concentration and the charge of species i, because the valency of the citrate ion is 3. Nevertheless, these citrate molecules cannot be removed, otherwise desorption occurs and a destabilization of the solutions is observed after several days or weeks.[21]

2.2. SANS Experiments. The experiments have been performed on the PAXY and PAXE spectrometers of the Laboratoire Léon Brillouin (CEA-CNRS) in the reactor Orphée (CE-Saclay, France). The neutron wavelength is $\lambda = 10$ Å, the detector distance is 3.2 m, which leads to a scattering vector q between 0.007 and 0.07 Å^{-1}. The contrast, i.e., the squared differences of density of scattering length, between the maghemite particles and the solvent are $C^2 = 56.7 \times 10^{20}$ cm^{-4} in H_2O and $C^2 = 0.36 \times 10^{20}$ cm^{-4} in D_2O, which is 150 times lower than that in H_2O. There is therefore no need for using D_2O, and the samples are analyzed in light water, despite its high incoherent scattering. The sample is put in a quartz cell, the thickness of which lies between 1 and 0.1 mm depending on the particle volume fraction. A standard data treatment is applied in order to subtract the scattering from the solvent and the quartz cell.[19,21] In all the SANS figures, the error bars are smaller than the symbols.

The cross section per volume $d\Sigma/d\Omega$ (later noted $I(q)$ for practicality) may be written

$$\frac{d\Sigma}{d\Omega}(\text{cm}^{-1}) = I(q) = nV_w^2C^2P(q)S(q,\Phi) = \Phi V_w C^2 P(q) S(q,\Phi)$$

where n is the number of particles per volume, V_w is the mean particle volume, C^2 is the contrast, and Φ is the particle volume fraction. $P(q)$ is related to the geometry of the particles while $S(q,\Phi)$ is related to the interactions between particles. In our stable colloidal solution, we assume that, if no aggregation occurs, the form factor $P(q)$ is the one of a spherical particle and is independent of the volume fraction Φ. At low volume fraction (1%), $P(q)$ is given by $1(q)/\Phi V_w C^2$. We thus can estimate the experimental structure factor $S(q,\Phi)$ by $S(q,\Phi_1) = (I(\Phi_1)/\Phi_1)/(I(\Phi_2)/\Phi_2)$ with $\Phi_1 > \Phi_2$ and $\Phi_2 \leq 1\%$. For low q values, $S(q,\Phi)$ is related to the compressibility χ by

$$\lim_{q\to 0} S(q,\Phi) = \chi = \left(\frac{k_B T}{V_w}\frac{\partial\Phi}{\partial\pi}\right)$$

where π is the osmotic pressure, T the temperature in Kelvin, and k_B the Boltzmann constant.

Table 2. List of the Solutions Studied by SANS at 30 °C[a]

sample A		sample B		sample C	
Φ (%)	c_{sel} (mol/L)	Φ (%)	c_{sel} (mol/L)	Φ (%)	c_{sel} (mol/L)
0.5	0*	0.4	0	0.5	0*
1	0	0.9	0*		
1	0.4				
1	0.53				
2	0*				
3	0*				
4.2	0	4.2	0	4.7	0
4.2	0.3	4.2	0.3	4.7	0.156
4.2	0.4	4.2	0.35	4.7	0.29
4.2	0.53	4.2	0.41	4.7	0.31
11	0	8.5	0	5.6	0
11	0.11	8.5	0.11		
11	0.22	8.5	0.22		
11	0.34	8.5	0.25		
11	0.37	8.5	0.3		

[a] Φ is the particle volume fraction, c_{sel} is the concentration of added NaCl. All these solutions, except these with a asterisk, have been studied at various temperatures between 30 and 8 °C.

2.3. Phase Diagrams. In the present work, we induce phase separations through a NaCl addition or a decrease of temperature. Some studies by optical microscopy (magnification 40×) are first performed in order to determine the phase separation thresholds and to determine the nature of the phases. The phase diagram is then built. For phase separations induced by NaCl addition, the salt is added as a powder under stirring and we let the obtained diphasic samples sediment during 2 days before any characterization. To build up the phase diagrams as a function of temperature T, the sample cells are put in a water/ethylene glycol bath, the temperature of which is controlled between −10 and 40 °C (±0.05 °C). The temperature is then decreased from 30 °C to the desired temperature, and the samples are kept in the bath during 8 h. The characterization procedures of the coexisting phases are the same for both diagrams. The phases are separated and the volume fraction measured. It must be stressed that the bottom phase is usually very concentrated and thus extremely viscous and that its volume is very small (typically 10 to 50 μL for a total volume around 0.5 mL). Important errors thus follow in the determination of the concentration of the concentrated phases.

3. Scattering Results for Addition of Salt at Constant Temperature

3.1. Experimental Data. The addition of electrolyte screens the repulsion between particles, which may induce a separation of the colloidal solutions in two phases above a given threshold, if attractions become predominant. As long as this threshold is not reached, SANS experiments allow studying the evolution of interactions.

Three samples, A, B, and C, which differ from one another in their mean particle size, are studied. The volume fractions and salt concentrations used in the experiments are all given in Table 2. As an example, the scattered intensity $I(q)$ of sample A at $T = 30$ °C is plotted in Figure 2 for different added NaCl concentrations. At

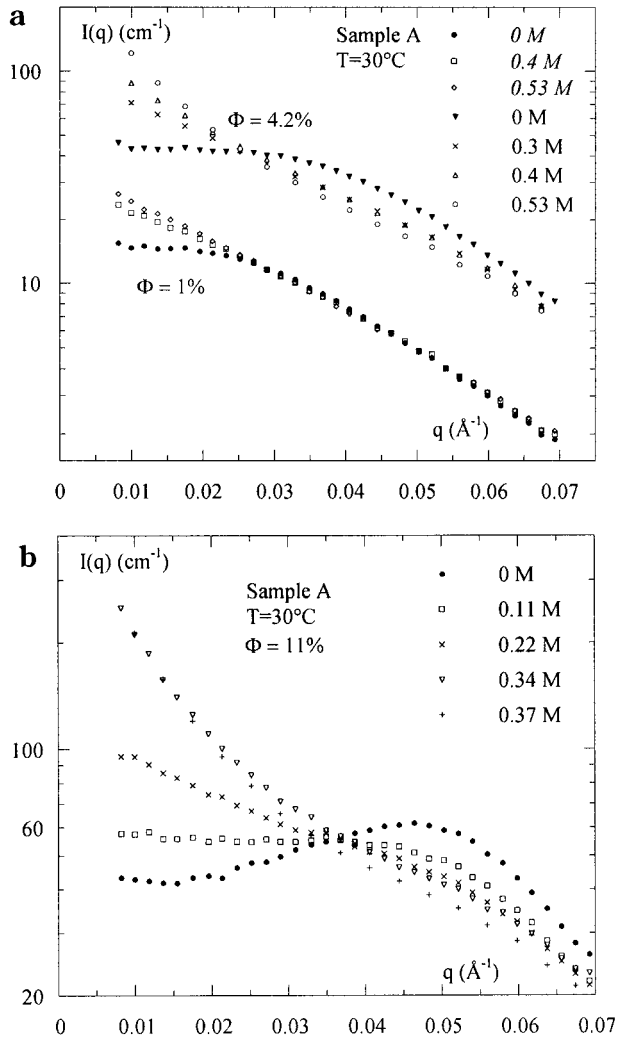

Figure 2. Scattered intensity $I(q)$ for sample A at $T = 30$ °C for several NaCl concentrations (given in the legend): (a) $\Phi = 1\%$ (italic legend) and $\Phi = 4.2\%$; (b) $\Phi = 11\%$.

low volume fraction ($\Phi = 1\%$), the intensity increases at low q if NaCl increases (Figure 2a). For higher volume fractions (4 and 11%), there is in addition a decrease of the intensity for large q (Figure 2). At $\Phi = 11\%$, the peak observed in the sample with no added salt progressively smears out. This is easier seen in Figure 3, which plots the structure factor $S(q)$ for samples A (Figure 3a) and B (Figure 3b): the peak decreases while adding salt and disappears. This peak, which characterizes the liquid structure of the solution, is due to the repulsion and, consequently, disappears if electrolyte is added. The high increase of intensity for small q shows that the compressibility increases if electrolyte is added. This is consistent with the increase of the proportion of attractions in the interparticle potential.

3.2. Determination of the Second Virial Coefficient A_2. This evolution can be quantified by deducing the second virial coefficient A_2 of the osmotic pressure π. For small q and small Φ, a first-order development is possible and we can write

$$\left(\frac{\Phi}{I}\right)_{q\to 0} = \frac{1}{C^2}\left(\frac{1}{k_B T}\frac{\partial \pi}{\partial \Phi}\right) = \left(\frac{\Phi}{I}\right)_{\substack{q\to 0\\ \Phi\to 0}} (1 + 2M_w A_2 \rho_m \Phi) = \frac{1}{V_w C^2} + \frac{2{\rho_m}^2 N_A}{C^2} A_2 \Phi \quad (2)$$

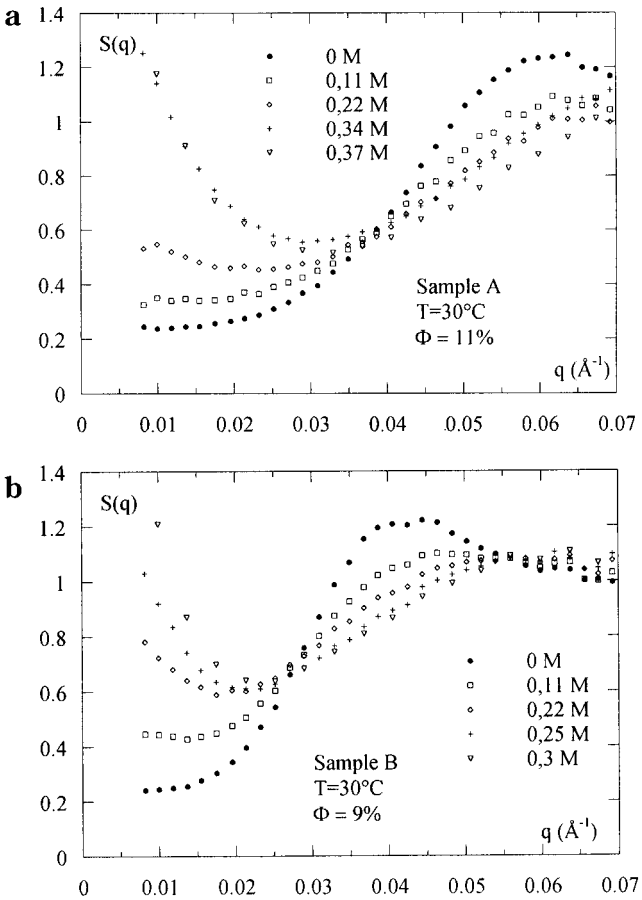

Figure 3. Structure factor $S(q)$ at $T = 30$ °C for several NaCl concentrations (given in the legend): (a) sample A with $\Phi = 11\%$; (b) sample B with $\Phi = 9\%$.

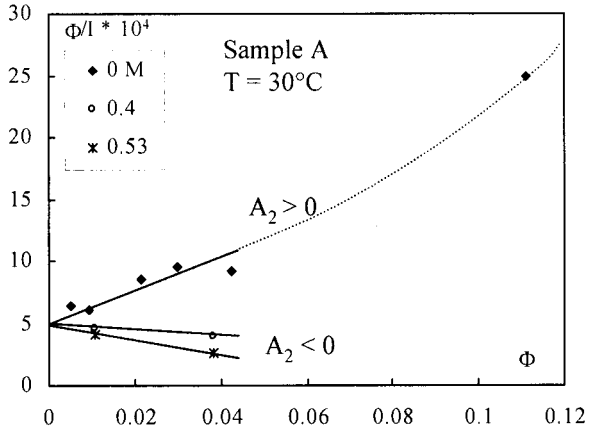

Figure 4. Φ/I as a function of Φ for sample A. $T = 30$ °C and NaCl concentrations are given in the legend.

where Φ is the particle volume fraction, C^2 is the contrast, $\rho_m = 5.03$ g/cm^3 is the mass per volume, N_A the Avogadro number, and thus $M_w = \rho_m N_A V_w$ is the mean particle weight. The particle volume V_w and the coefficient A_2 can thus be derived from the plot of $(\Phi/I)_{q=0}$ as a function of Φ, the ordinate being obtained by a linear extrapolation to $q = 0$ of $(\Phi/I) = f(q)$ for $q < R_g^{-1}$ (R_g is the radius of gyration).

Figure 4 presents the plot obtained for sample A for different added salt concentrations at $T = 30$ °C. For no added salt, it shows that A_2 is positive, thus that the repulsion is predominant ($A_2 = 3.6 \times 10^{-6}$ mol·cm^3·g^{-2}, see Table 1). As NaCl increases, A_2 becomes negative. In Figure 4, the highest salt concentration is very close to

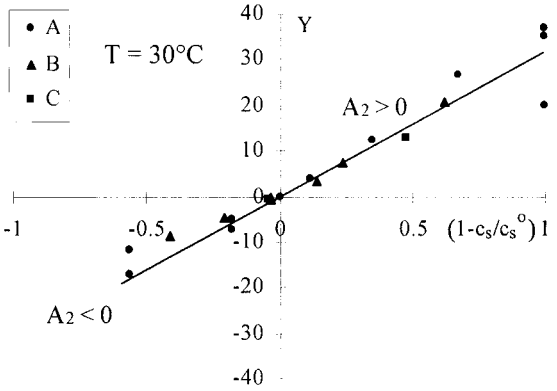

Figure 5. $Y = ((\Phi/I) - (1/V_w\Delta\rho^2))(V_w\Delta\rho^2/\Phi)$ as a function of $1 - c_s/c_s^o$ (see text and eq 4) for $T = 30$ °C. The results for the three samples A, B, and C in all the conditions of added NaCl (see Table 2) are reported on this graph.

the destabilization threshold, which equals 0.56 mol/L. It can be checked in this figure that the value $(\Phi/I)_{q=0}$, extrapolated at $\Phi = 0$, is independent of NaCl concentration. As $(\Phi/I)_{q=0}$ is inversely proportional to the volume V_w of the scattering objects, we can conclude that *no aggregates are formed when approaching the separation threshold* ($V_w = 3 \times 10^5$ Å^3, see Table 1). The scattering objects are thus the isolated particles and the form factor $P(q)$ does not depend on the added salt concentration: the changes observed correspond to an evolution of the interparticle interactions.

Looking more closely at these data, we noticed that the quantity $(\Phi/I)_{q\to 0} - 1/V_wC^2$, proportional to A_2, depends linearly on the ionic strength c_s for a given volume fraction, with a slope $-\alpha$

$$\left(\frac{\Phi}{I}\right)_{q\to 0} - \frac{1}{V_wC^2} = \frac{2\rho_m{}^2N_A}{C^2}A_2\Phi = -\alpha(c_s - c_s{}^o) \quad (3)$$

where the parameter $c_s{}^o$ corresponds to the concentration for which the coefficient A_2 is zero at $T = 30$ °C. The parameter $\alpha c_s{}^o$ is found to vary as Φ/V_w, i.e., the number of particles, $\alpha c_s{}^o(V_wC^2/\Phi)$, is thus a constant. The plot of $Y = V_wC^2/\Phi[\Phi/I - 1/V_wC^2]$ as a function of $(1 - c_s/c_s{}^o)$ (see Figure 5)

$$Y = 2\rho_mM_wA_2 = 2\rho_m{}^2N_AV_wA_2 = \alpha c_s{}^o\frac{V_wC^2}{\Phi}\left(1 - \frac{c_s}{c_s{}^o}\right) \quad (4)$$

then clearly proves that $Y = 2\rho_m{}^2N_AV_wA_2$ is proportional to $(1 - c_s/c_s{}^o)$, with a proportionality constant equal to 33 ± 3 at 30 °C. We stress the fact that $A_2 = 0$ at the origin of the axes ($c_s{}^o = c_s$). It follows from eq 4 that the coefficient A_2 for $c_s = 0$ at $T = 30$ °C is given by

$$A_2(c_s{=}0) = \frac{C^2}{2\rho_m{}^2N_A}\frac{\alpha c_s{}^o}{\Phi} \quad (5)$$

a formula which leads to the values of Table 1. These values extrapolated for different salt concentrations are in good agreement with those previously directly determined with no added salt at room temperature: $(1.6 \pm 0.2) \times 10^{-6}$ mol·cm^3·g^{-2} for a sample with $\sigma = 0.15$ and $d_o = 77$ Å [21] and 0.5×10^{-6} mol·cm^3·g^{-2} for polydisperse maghemite particles ($\sigma = 0.3$, $d_o = 100$ Å).[25] They moreover show a pronounced size dependence: the potential is less repulsive (A_2 decreases) while increasing the mean particle diameter. This is related to the evolution of the interparticle interactions with particle size: in a representation of potential versus r/d_o (r being the distance between particle centers), van der Waals attractions are independent of d_o while the electrostatic repulsion decreases for larger d_o.

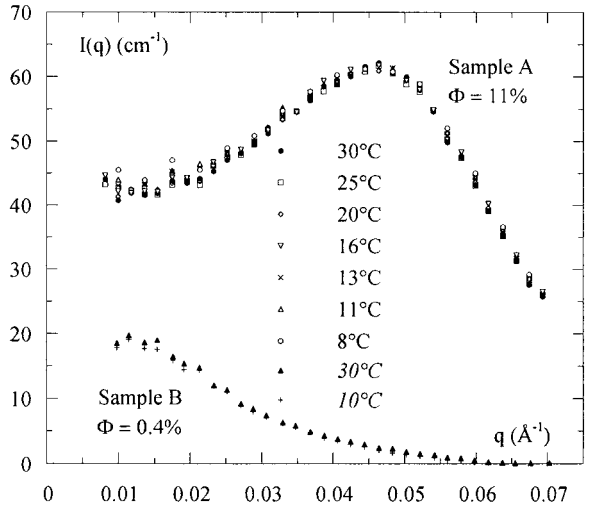

Figure 6. Scattered intensity for several temperatures without added NaCl. The upper curves correspond to sample A with $\Phi = 11\%$ and the lower curves (italic legend) correspond to sample B with $\Phi = 0.4\%$.

4. Scattering Results for Decreasing Temperature

4.1. Experimental Data. The three samples of Table 1 were studied for various temperatures ranging from 30 °C down to 8 °C without and with added salt. Table 2 lists the characteristics of the solutions studied in these experiments.

If no salt is added, the samples remain macroscopically stable for all temperatures until freezing of the solvent (around −10 °C). Moreover, SANS experiments show that there is no influence of temperature on the spectra. Figure 6 presents two examples: sample A at $\Phi = 11\%$ and sample B at $\Phi = 0.4\%$. These spectra prove that temperature influences neither the sample structure factor, i.e., the interparticle interaction without added salt, nor the form factor.

If salt is previously added, the intensity at small q increases while decreasing T, as shown in Figure 7 for sample A at $\Phi = 4\%$. If a phase separation occurs while decreasing temperature, this is experimentally easily seen because the intensity at small q decreases, contrary to what is expected. Indeed, if the sample has been destabilized, the dense phase sediments at the bottom of the cell and the measured spectrum corresponds to the dilute phase, leading to a smaller intensity. In Figure 7, the solution with [NaCl] = 0.3 mol/L remains stable in the whole temperature range studied, whereas the solution with [NaCl] = 0.53 mol/L at 30 °C is very close to the destabilization threshold. These results demonstrate that a temperature decrease has an influence analogous to a NaCl increase.

4.2. Determination of the Second Virial Coefficient A_2. If we again apply the same procedure as in section 3.2., we also find that $(\Phi/I)_{q\to 0} - 1/(V_w\Delta\rho^2)$ is linear with c_s (see eq 3). Figure 8 then plots Y as a function of $(1 - c_s/c_s{}^o)$ (see eq 4) and shows that $\alpha c_s{}^o(V_wC^2/\Phi) = 33 \pm 3$ is

(25) Bacri, J. C.; Boué, F.; Cabuil, V.; Perzynski, R. *Colloids Surf., A* **1993**, *80*, 11.

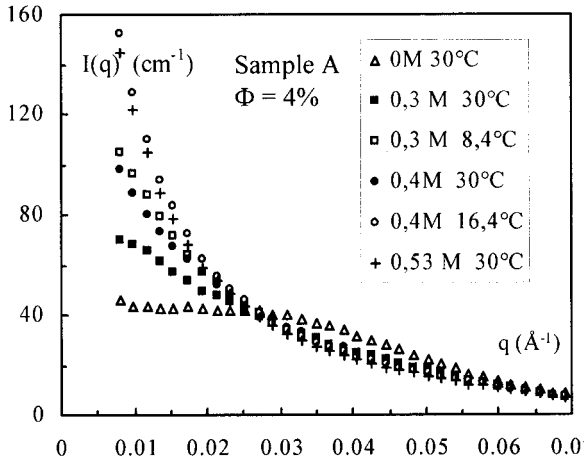

Figure 7. Influence of temperature on the scattered intensity for sample A with added NaCl (Φ = 4%). Ionic strength and temperature are given in the legend. The destabilization occurs between 16.4 and 13.5 °C at 0.4 mol/L and between 30 and 25 °C at 0.53 mol/L.

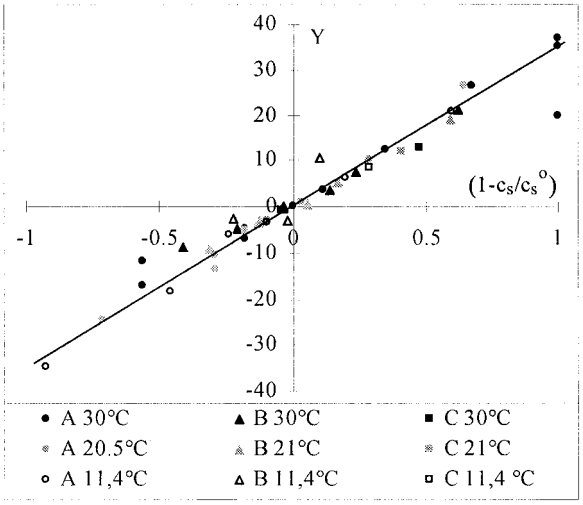

Figure 8. $Y = ((\Phi/I) - (1/V_w\Delta\rho^2))(V_w\Delta\rho^2/\Phi)$ as a function of $1 - c_s/c_s^o$ (see text and eq 4). Temperatures and symbols are given in the legend. On this graph are reported the results for the three samples A, B, and C for all salt concentrations of Table 2 and three temperatures.

a constant for all samples and temperatures. This means that the coefficient αc_s^o is independent of T. We determine that

$$\alpha\frac{V_w C^2}{\Phi} = \frac{33}{c_s^o} = 1.5_{\pm 0.15}(T - 273) + 145_{\pm 5}$$

with T in kelvin. It means that c_s^o decreases, i.e., that A_2 is zero for lower salt concentration, if temperature is lowered. Such an evolution is consistent with the increase of attractive interactions induced by the temperature decrease. It leads for A_2 to the empirical expression

$$A_2 = \frac{C^2}{2\rho_m{}^2 N_A}\frac{\alpha c_s^o}{\Phi}\left(1 - \frac{c_s}{c_s^o}\right) = \frac{1.06}{V_w}[1 - (16.7 - 0.045T)c_s] \quad (6)$$

with T in K, c_s in mol/L, V_w in Å^3, and A_2 in mol·cm^3·g^{-2}. From this relation for A_2, we can derive an expression for the osmotic pressure π of the solution

$$\pi = k_B T\frac{\Phi}{V_w}(1 + \rho^2 N_A V_w A_2\Phi) = \frac{(1.38 \times 10^7)\Phi T}{V_w}[1 + 16.5\Phi(1 - (16.7 - 0.045T)c_s)] \quad (7)$$

with T in K, c_s in mol/L, and V_w in Å^3. This empirical expression characterizes aqueous ferrofluids at pH 7 in the one-phase region, in the explored ranges of temperature, of electrolyte concentration and particle sizes. As the osmotic pressure π is developed to the second order, it is important to notice that the formula of eq 7 is valid for small volume fractions (Φ < 5%) only.

This calculated osmotic pressure is consistent with direct π measurements,[26] performed with a membrane osmometer, which measures the difference of pressure between a solution and its dialysis bath (see Figure 9). The ferrofluid used in ref 26 is of the same kind as the ferrofluids studied here; however the particles are more polydisperse (d_o = 85 Å and σ = 0.4). The citrate concentration, which contributes to the initial ionic strength (without added NaCl), is fixed by dialysis to 0.01 mol/L, a value which is lower than the citrate concentration in our samples A, B, and C (more than 0.04 mol/L, see section 2.1.). The two parameters c_s and V_W are needed in eq 7. The c_s concentration is zero because no salt has been added. As the volume V_W has not been determined from SANS experiments, we determine it from the fit. This leads to $V_W = 11 \times 10^5$ Å^3, a value close to the volume $V_W = 13.6 \times 10^5$ Å^3 of a polydisperse sample similar to the one used here.[25] Direct π measurements and values calculated from SANS results are thus in good agreement.

In conclusion, it follows clearly from eq 7 that a decrease of temperature and an electrolyte addition qualitatively have the same influence: the osmotic pressure decreases because the repulsion between particles decreases. Under a given pressure threshold, which depends on particle size, volume fraction, and temperature, the ferrofluid sample separates in two phases.

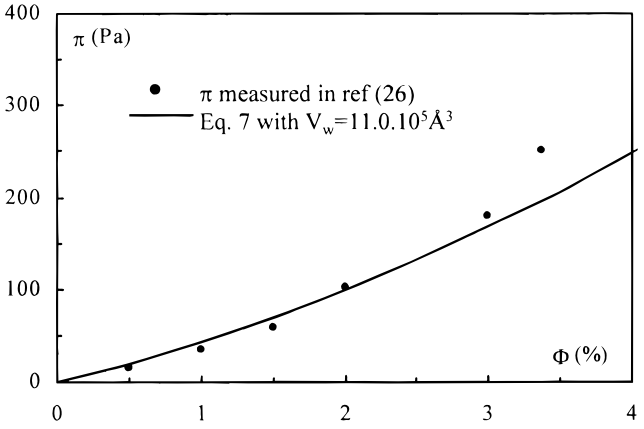

Figure 9. Comparison of the measured osmotic pressure π (from ref 26) with the values calculated from eq 7 for two different volumes V_w (see text for details). The points correspond to the π measurements with a stable polydisperse sample (d_o = 8.5 nm, σ = 0.4) with no added salt.

5. Macroscopic Phase Diagrams

5.1. Experimental Results. Beyond the threshold, the sample separates in two phases and macroscopic characterizations replace microscopic SANS studies. Phase diagrams are built up and plotted in Figure 10 for sample

(26) Cousin, F.; Cabuil, V. *J. Mol. Liq.* **1999**, *83*, 203.

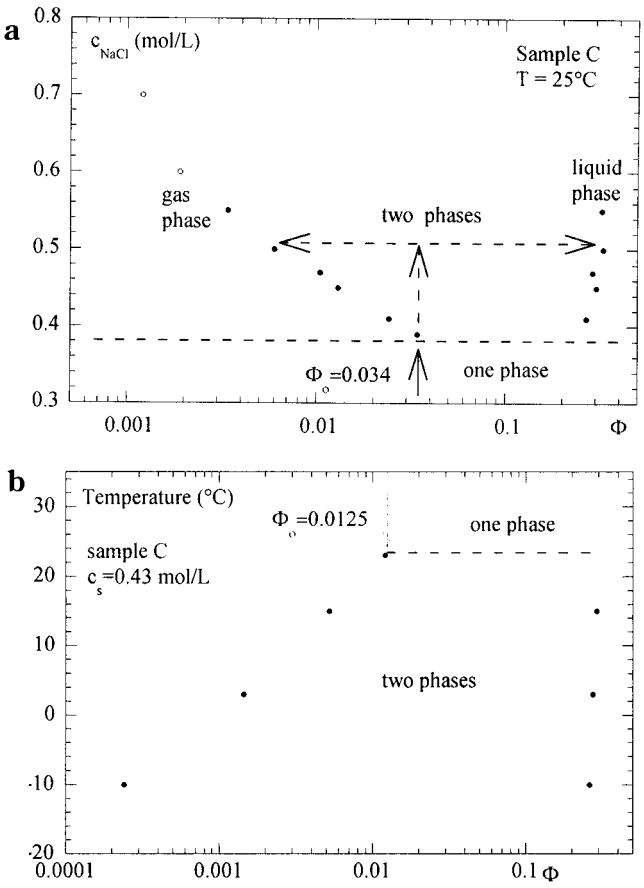

Figure 10. Phases diagrams for sample C. The destabilizing parameter is either NaCl (a) or temperature T (b). Φ_o is the initial volume fraction, and the dotted line corresponds to the destabilization threshold. The black dots correspond to a liquid dense phase and the white dots to a solid dense phase.

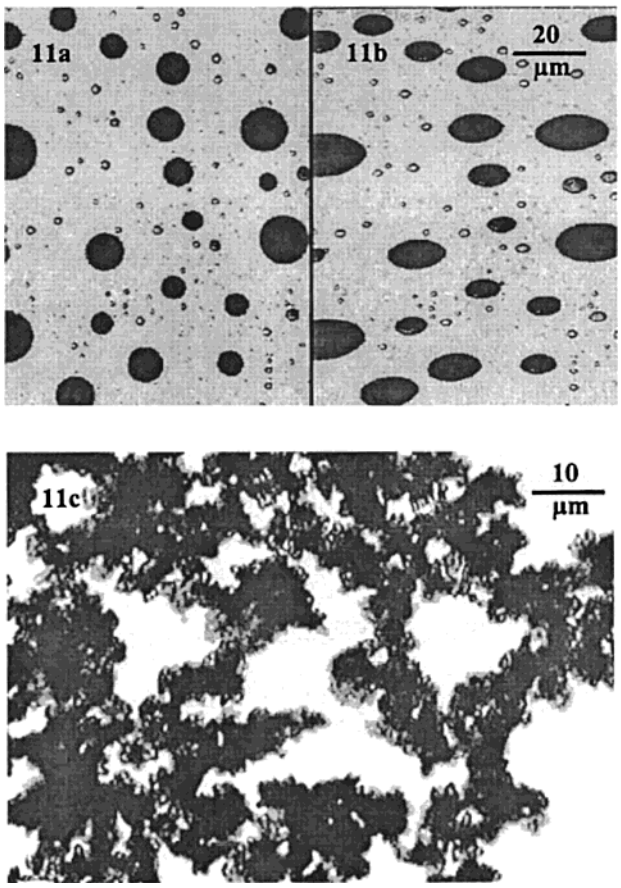

Figure 11. Optical microscopy photographs of two-phase samples: (a) gas−liquid-like transitions; (b) the same photograph as (a) with an horizontal applied magnetic field; (c) gas−solid-like transition.

C. Figure 10a shows a diagram [NaCl] = $f(\Phi)$ for T = 25 °C and Figure 10b a diagram $T = f(\Phi)$ for c_s = 0.43 mol/L. It has to be noticed that these observed phase transitions are always reversible: decreasing NaCl or increasing temperature afterward leads back to a monophasic sample.

Let us discuss the *diagram [NaCl]* = $f(\Phi)$. It is important to specify first that the ordinate [NaCl] is the appropriate parameter, given that chemical titrations have shown that it is the same in both coexisting phases.[21] Above a threshold, the solution, characterized by the particle volume fraction Φ_o, separates into a dilute phase ($\Phi < \Phi_o$) and a dense phase, highly concentrated (see Figure 10a). Note that it is not possible to determine the concentration of the dense phase near the destabilization threshold, because the volume of the concentrated liquid phase is too small. Observations with optical microscopy clearly show that this dense phase is liquid: it looks like spherical drops, which may be elongated along an applied magnetic field H (Figure 11a,b). If H is removed, drops recover their initial spherical shape.[18] However, as specified in Figure 10a, for high NaCl concentrations, a precipitated solid phase forms sediments at the bottom of the tube (see open symbols in Figure 10a). Contrary to the liquid phase, the latter phase can no longer be distorted with the applied field and behaves like a solid under a microscope (see Figure 11c).

The *diagram* $T = f(\Phi)$ is built for sample C. Separation with temperature can be observed for NaCl concentrations close to the NaCl threshold at room temperature. In Figure 10b, for [NaCl] = 0.43 mol/L, sample C separates below T = 23 °C. The microscopic observation is the same as with NaCl: a dilute and a concentrated liquid phase coexist. It is however important to note here that the rate of the temperature decrease has a deep influence on the nature of the concentrated phase. At low rate (2 °C/h), the phase at the bottom of the tube looks liquid, whereas, at high rate (15 mn to reach the set temperature), it looks solid. In both cases, the concentration of the dilute phase is the same, within the limit of titration accuracy. However, if the sediment looks solid, i.e., like Figure 11c, it is a macroscopic structure of holes full of dilute phase that does not allow titrating the solid phase.

5.2. Nature of the Transitions. These results raise the problem of the metastability of the observed phenomena: Do the phases observed always correspond to an equilibrium state? Experiments combining T and NaCl enlighten this question. When two-phase samples (separated by adding salt at room temperature), for which the bottom phase looks like a solid, are heated, they may become monophasic if their temperature threshold is not too high (otherwise water evaporates). A further slow decrease of temperature then leads to liquid drops of the concentrated phase. According to this result, associated with the influence of the rate of the temperature decrease, one is led to assume that some of the data identified as a solid phase actually correspond to metastable situations. Such observations of metastability have moreover been reported in other experimental works.[11]

Let us discuss the concentration of the dense phase formed when a phase separation occurs. If the dense phase clearly looks liquid, its volume fraction Φ_c of magnetic material always lies between 20 and 30%. However, this volume fraction does not take into account the citrate

molecules adsorbed on the surface. The thickness of the citrate shell being around 5 Å, this leads, for particles with $d = 8$ nm and $\Phi_c = 20\%$ to 30% to an effective volume fraction $\Phi_c^{eff} = 30-40\%$. As the NaCl concentration is very high in such phases, the Debye length is very short and the solution is equivalent to a system of hard spheres (maghemite + citrate shell). As such a system is supposed to become solid above $\Phi_c^{eff} = 50\%$,[2] the volume fractions Φ_c^{eff} measured for the concentrated phase are actually consistent with a liquid structure. If the dense phase does not look liquid, the sediment is a mixture of the dense phase and of the dilute one, which are impossible to separate. The dense phase concentration thus cannot be determined. If corresponding to nonequilibrium states, this macro-organization of the sediment may result from a too violent quench when quickly decreasing temperature or when adding NaCl as a solid powder. This quench does not allow the solid phase to organize and properly pack at macroscopic scale. Under the same experimental conditions, a slow decrease of temperature leading to gas−liquid transitions, one may assume that this macro-organized sediment is metastable.

On the other hand, it is not possible to experimentally demonstrate that, in our systems, all the phase transitions that look gas−solid are metastable. Some experiments have been performed with a new method to prepare the samples: osmotic compression. The pressure is imposed to the solution (placed in a dialysis tube) with a polymer, which imposes a known osmotic pressure as a function of its concentration. The salt concentration and the temperature can be controlled. After several weeks, the equilibrium is reached and the colloidal dispersion inside the dialysis tube can be characterized. Some preliminary results show that, if [citrate] = 0.01 mol/L, a fluid−solid transition is observed around $\Phi = 25\%$. In this system, the equivalent hard sphere diameter, calculated taking into account the maghemite core, the citrate shell, and the Debye length (no longer negligible here), leads to $\Phi_c^{eff} = 47\%$, a value which is very close from the hard sphere transition which occurs at 50%.[27] Moreover, some scattering experiments show that these samples present strong repulsive interactions between particles and demonstrate that the solid-phase exists.[27] As the particles are not monodisperse enough, this solid is not a crystal: it is a glass. In the future, osmotic compression may be a suitable "soft" method to investigate in detail the gas−solid region and to complete the phase diagram.

6. $\pi-\Phi$ Diagram

Combining the π formula (eq 7) obtained from SANS experiments and the phase diagrams experimentally determined (Figure 10), one may build up a general $\pi = f(\Phi)$ phase diagram similar to the schematic diagram of Figure 1.

Using eq 7, which is valid in the low volume fraction limit, we build the dilute branch of the $\pi-\Phi$ diagram. As the pressure is the same in both coexisting phases, the branch corresponding to the dense liquid phase may also be deduced. The diagrams obtained in this way for samples A and C at room temperature and for sample C with $c_s =$ 0.43 mol/L are plotted in Figure 12 in a reduced presentation. For the highest π values, the separation is gas−liquid like. This is consistent with the supposed critical phenomena observed for sample C at $\Phi = 5.6\%$ for $T =$ 25 °C.[21] At very low osmotic pressure, the separation may correspond to a gas−solid one (see comments of section 5).

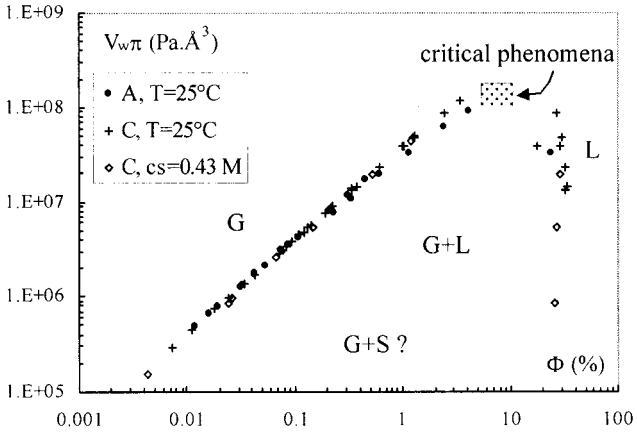

Figure 12. $V_w\pi-\Phi$ phase diagram which groups diagrams as a function of [NaCl] and as a function of T, as indicated in the legend: G, gas; L, liquid; S, solid.

This experimental phase diagram seems to correspond to the situation plotted in Figure 1, i.e., to a system where the attractions are long-ranged relative to the repulsion.[7] This is consistent with the fact that, due to the very strong ionic strength in the solution, the range of the repulsive interaction is very short, but nevertheless sufficient to stabilize the dispersions. Moreover, as predicted in the theoretical work of ref 15, the gas−liquid transitions are observed in a narrow range of parameters and increasing ionic strength is equivalent to decrease temperature. However, a detailed comparison to ref 15 shows several discrepancies. First, we do not observe the predicted irreversible coagulation, whatever the NaCl concentration. This irreversible coagulation should result from the primary minimum in the interparticle potential due to van der Waals forces. It is probably avoided in our experimental system by the shell of citrate molecules adsorbed on the particle surface that prevents the particles from coming too close. Second, gas−liquid transitions are always observed for 4 nm < d_o <12 nm. It is in contradiction with the authors' predictions of a particle size threshold around 500 nm under which no gas−liquid transitions can be observed. This discrepancy may be due to a structural surface charge which is very high[16] and which probably invalidates the hypothesis of a low surface potential.

The observation of a gas−liquid transition is also in good agreement with theoretical works on dipolar systems. Several authors[28,29] have performed Monte Carlo simulations for such systems, varying the proportion of anisotropic interactions compared to isotropic attractions. Both studies lead to the same conclusion. While varying dipolar interactions, the system may destabilize in two different ways, leading either to a gas−liquid coexistence for weak dipolar interactions or to a chaining of the particles for strong dipolar interactions. The system indeed choses the most favorable solution given its interparticle interactions. In agreement with Monte Carlo simulation results, we do not detect any particle chaining and on the contrary observe a destabilization in a gas phase and a liquid phase.

7. Conclusions

Monodisperse ferrofluids at pH 7 are electrostatically stabilized dispersions of nanoparticles, the phase behavior of which is seldom studied. If the interparticle repulsion is reduced by a salt addition or by a temperature decrease,

(27) Cousin, F.; Cabuil, V. Accepted in *Prog. Colloid Polym. Sci.*

(28) van Leeuwen, M. E.; Smit, B. *Phys. Rev. Lett.* **1993**, *71*, 3991.
(29) Stevens, M. J.; Grest, G. S. *Phys. Rev. E* **1995**, *51*, 5976.

gas−liquid-like phase transitions are observed. Such a phase behavior is scarcely reported in such systems, which more often only present gas−solid transitions. Nevertheless, here, the observation of gas−solid transitions is disturbed by metastability phenomena.

Small-angle neutron scattering experiments on monophasic samples demonstrate that increasing NaCl and decreasing temperature are qualitatively equivalent. These experiments also enable the determination of a phenomenological expression for the osmotic pressure $\pi = f(c_s,T,V_w)$, in good agreement with measurements directly performed with an osmometer.[26] The association of both SANS and macroscopic measurements of stability limits allows us to build a $\pi-\Phi$ phase diagram. The phase behavior of these colloidal solutions is in qualitative agreement with predictions concerning such electrostatically stabilized systems[15] and with predictions for systems with weak dipolar interactions.[28,29]

It would now be interesting to complete this phase diagram by precisely determining the critical point, which has been approached with several samples, by looking for a triple point, and by determining the solid branch of the phase diagram. As shown in preliminary results, the osmotic compression method could be convenient to elucidate the metastability questions. For a further study, it would be necessary to directly work on more concentrated dispersions ($\Phi > 10\%$). However, it raises several difficulties, in particular because of their strong absorption of light. Finally, in concentrated samples, specific behaviors may be observed due to the magnetic dipolar interactions. If the particles are large enough ($d > 8$ nm), these interactions become significant because the particles are close to each other. It may induce a chaining of the particles without magnetic field and some displacements of the boundaries in the phase diagram under magnetic field.

Acknowledgment. We thank F. Cousin for fruitful discussions, in particular for preliminary results of experiments currently under process. This work was supported by DRET/DGA.

LA000053U